

Article

Design and Optimization of a Resonant Micro-Optic Gyroscope Based on a Transmissive Silica Waveguide Resonator

Wei Zhang ^{1,2,*}, Wenyao Liu ^{1,2}, Huiting Guo ^{1,2}, Jun Tang ^{1,2} and Jun Liu ^{1,2,*}

¹ Shanxi Province Key Laboratory of Quantum Sensing and Precision Measurement, North University of China, Taiyuan 030051, China

² Key Laboratory of Electronic Testing Technology, School of Instrument and Electronics, North University of China, Taiyuan 030051, China

* Correspondence: zbdxzhangwei@163.com (W.Z.); liuj@nuc.edu.cn (J.L.)

Abstract: In order to optimize the performance of a resonant micro-optic gyroscope, a well-designed transmissive structure, which was obtained by optimizing the transmission coefficient of a coupler was used as the core component of a planar waveguide optical gyroscope. By analyzing the relationship between the resonator's transmission coefficient and the gyroscope's scale factor, the optical waveguide resonator sensing element with optimal parameters for the resonant micro-optic gyroscope was obtained. A scale factor of 1.34 mV/°/s was achieved using an open-loop system, and a bias stability of 183.7 °/h over a one-hour test was successfully demonstrated.

Keywords: resonant micro-optic gyroscope; transmissive resonator; waveguides



Citation: Zhang, W.; Liu, W.; Guo, H.; Tang, J.; Liu, J. Design and Optimization of a Resonant Micro-Optic Gyroscope Based on a Transmissive Silica Waveguide Resonator. *Electronics* **2022**, *11*, 3355. <https://doi.org/10.3390/electronics11203355>

Academic Editor: Giovanni Andrea Casula

Received: 22 September 2022

Accepted: 14 October 2022

Published: 18 October 2022

Publisher's Note: MDPI stays neutral with regard to jurisdictional claims in published maps and institutional affiliations.



Copyright: © 2022 by the authors. Licensee MDPI, Basel, Switzerland. This article is an open access article distributed under the terms and conditions of the Creative Commons Attribution (CC BY) license (<https://creativecommons.org/licenses/by/4.0/>).

1. Introduction

A resonant micro-optic gyroscope is a novel optoelectronic hybrid integrated sensor with great potential to realize miniaturized all-solid-state devices and monolithic device integration [1,2]. Benefitting from the mature process of integrated circuits and planar light waveguide circuits, the realization of all integrated resonant micro-optic gyroscopes on a single chip has been proposed for years and is developing rapidly [3,4]. Because a waveguide ring resonator is the core sensing element of a gyroscope, its performance directly determines the precision of the gyroscope. The design and fabrication of a high quality resonator has become an important research topic for optical waveguide gyroscopes.

A number of parameters are directly related to a gyroscope's performance, including the quality factor and effective area of a resonator. In view of the development trend of gyroscope miniaturization and integration, the question of how to optimize the parameters of a resonator of a finite size to improve the performance of a gyroscope is urgent. In recent years, research on resonators for resonant optical gyroscopes has developed rapidly [5–13]. Vannahme et al. fabricated a 6 cm diameter ring resonator on a LiNbO₃ substrate with a Q factor of 2.4×10^6 [14].

Ciminelli et al. fabricated an InP-based spiral resonator with a quality factor (Q factor) of 6×10^5 and an effective area of 10 mm²; the resolution of the gyroscope was 150 °/h [15]. Feng et al. fabricated a silica waveguide ring resonator with a Q factor of 1.4×10^7 , for which a long-term bias stability of 0.013 °/s was reported [16].

Planar optical resonators include transmissive structures and reflective structures. Compared with a reflective resonator, a transmissive resonator has one more coupling region, which introduces an additional coupling loss [17]; however, it seems to be more advantageous, not only in the sense that the structure is more symmetrical and reciprocal, but also in regard to the better suppression of the polarization fluctuation [18]. Moreover, circulators are not required when constructing the gyroscope system. Feng et al. designed a transmissive resonator optic gyroscope based on a silica waveguide ring resonator, for which the quality factor was 6.13×10^6 and the long-term bias stability was 0.22°/s [19].

In this paper, a resonant micro-optic gyroscope based on a transmissive silica waveguide ring resonator is reported. First, we established a physical model of the transmissive resonator, deduced the transfer function, analyzed the relationship between the resonator’s transmission coefficient and the gyroscope’s scale factor, and obtained the transmission coefficient at the maximum sensitivity. Then, micro-electro-mechanical-system (MEMS) processing was used to process the resonator. Finally, a gyroscope test system was built to carry out experiments. The experimental results agreed with the simulation results.

2. Principle and Simulation

A transmissive resonator consists of two straight waveguides and a circular waveguide. The structure diagram is shown in Figure 1a: E_{in} , $E_{through}$, and E_{drop} are the input port, through port, and drop port of the light fields, respectively. The light is divided into two parts when it arrives at coupling region 1: part of it travels to the through port, while the other couples into the circular waveguide. In the same way, E_1 will be spilt into two parts when arriving at coupling region 2: one part couples with a straight waveguide and then travels to the drop port, while the other continues propagating around the circular waveguide. When it meets the resonance conditions, the light of the ring resonator will reach a dynamic balance.

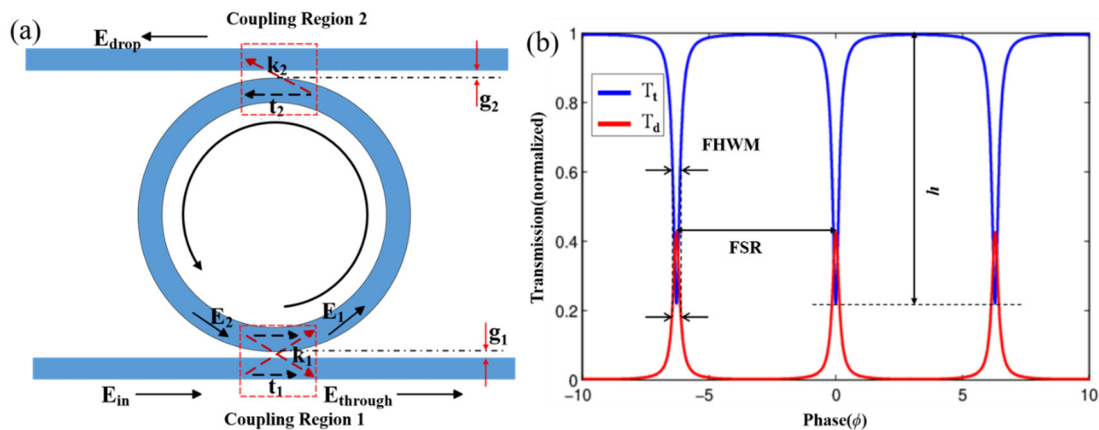


Figure 1. (a) Structural diagram of the transmissive ring resonator; (b) resonant spectrum of the resonator.

In Figure 1, $k_1, k_2, t_1,$ and t_2 are defined as the coupling coefficients and transmission coefficients of coupling region 1 and coupling region 2, respectively. In this paper, we assume that the coupling is lossless, in which case the parameters satisfy the following equation:

$$k_1^2 + t_1^2 = 1 \quad k_2^2 + t_2^2 = 1 \tag{1}$$

In Figure 1, g_1 and g_2 are the gaps between the straight waveguides and the circular waveguide, respectively. The transmission loss of the light during one cycle in the circular waveguide can be described using the round-trip loss factor a :

$$a = \sqrt{10^{-\alpha L/10}} \tag{2}$$

where α is the c-band transmission loss and ϕ is the round-trip phase of the resonator.

The transmission matrix method is used to analyze the transmission of light between the straight waveguides and the circular waveguide [20]; the relationship between the parameters can be expressed as follows:

$$\begin{pmatrix} E_{through} \\ E_1 \end{pmatrix} = \begin{pmatrix} t_1 & -ik_1 \\ -ik_1 & t_1 \end{pmatrix} \begin{pmatrix} E_{in} \\ E_2 \end{pmatrix} \tag{3}$$

$$E_{drop} = k_2 a^{1/2} e^{i\pi/2} e^{i\phi/2} E_1 \tag{4}$$

According to the above formulae, the normalized transfer function of the transmissive resonator can be represented as:

$$T_{through}(\phi) = \left| \frac{E_{through}}{E_{in}} \right|^2 = \frac{t_1^2 + a^2 t_2^2 - 2at_1 t_2 \cos \phi}{1 + a^2 t_1^2 t_2^2 - 2at_1 t_2 \cos \phi} \tag{5}$$

$$T_{drop}(\phi) = \left| \frac{E_{drop}}{E_{in}} \right|^2 = \frac{ak_1^2 k_2^2}{1 + a^2 t_1^2 t_2^2 - 2at_1 t_2 \cos \phi} \tag{6}$$

The resonance curve is plotted by the transfer function, as shown in Figure 1b. The blue curve T_t represents the resonant spectrum of the straight through port and the red curve T_d represents the resonant spectrum of the drop port. The full width at half maximum (FWHM), Δf , and the quality factor, Q , can be expressed as follows:

$$\Delta f = \frac{c}{n\pi L} \arccos \frac{2at_1 t_2}{1 + a^2 t_1^2 t_2^2} \tag{7}$$

$$Q = \frac{f}{\Delta f_{FWHM}} = \frac{n\pi L}{\lambda \arccos \frac{2at_1 t_2}{1 + a^2 t_1^2 t_2^2}} \tag{8}$$

where c is the speed of light in a vacuum, n is the refractive index of the waveguide, L is the perimeter of the circular waveguide, f is the resonant frequency, and λ is the operation wavelength in a vacuum.

The resonant depth, h , of the through port spectrum can be derived as follows:

$$h = \frac{T_{tmax} - T_{tmin}}{T_{tmax}} = 1 - \left(\frac{t_1 - at_2}{1 - at_1 t_2} \right)^2 \tag{9}$$

where T_{tmax} and T_{tmin} are the maximum and minimum of the transfer function of through port, respectively.

Equations (7) and (8) show that when the length of the circular resonator is fixed, the Q will be determined by the transmission coefficients t_1 and t_2 .

In a reflective resonant optical gyroscope, the best performance is achieved when the resonator is undercoupling and the resonant depth is 0.75 [13]. Therefore, in a transmissive resonator, the coupling loss from coupling region 2 can be approximately considered as a part of the loss in the reflective resonant. In this way, the round-trip loss factor, a , and the transmission coefficient, t_2 , can be regarded as a whole factor to simplify the analysis.

The slope, l , of the demodulation curve in the linear region is defined as a scale factor, which can be considered as the sensitivity of the gyroscope. The specific formula [21] is as follows:

$$l = \left. \frac{dI_{out}}{d\Delta f} \right|_{\Delta f=0} \tag{10}$$

$$I_{out} = I_{in} \left\{ \frac{t_1^2 + a^2 t_2^2 - 2at_1 t_2 \cos \frac{2\pi(\Delta f/2+f')}{FSR}}{1 + a^2 t_1^2 t_2^2 - 2at_1 t_2 \cos \frac{2\pi(\Delta f/2+f')}{FSR}} - \frac{t_1^2 + a^2 t_2^2 - 2at_1 t_2 \cos \frac{2\pi(\Delta f/2-f')}{FSR}}{1 + a^2 t_1^2 t_2^2 - 2at_1 t_2 \cos \frac{2\pi(\Delta f/2-f')}{FSR}} \right\} \tag{11}$$

where I_{in} , I_{out} represent the input and output light intensity of the photodetector, respectively. FSR represents the free spectrum width of the resonance curve, as shown in Figure 1b.

In this article, the diameter of the circular waveguide is 6 cm. The experimental test results show that the c-band transmission loss, α , of the silica optical waveguide is 0.017 dB/cm.

In combination with Equations (9) to (11), we can calculate that $t_1 = 0.9798$ and $t_2 = 0.9759$ when the slope of the demodulation curve is at its maximum at the resonant frequency point, and the corresponding gyroscope sensitivity is at its maximum at this time.

In this case, we only need to design the gaps between the straight waveguides and the circular waveguide to match the above transmission coefficient. Then, $g_1 = 6.9 \mu\text{m}$ and $g_2 = 6.7 \mu\text{m}$ can be obtained through the beam propagation method (BPM) simulation.

3. Design and Fabrication

A transmissive ring resonator was fabricated on a silicon substrate (Figure 2). The refractive indices of the core and the overlay were $n_1 = 1.456$ and $n_2 = 1.445$, respectively. First, the SiO_2 was thermally grown as the bottom cladding layer. Second, a $6 \mu\text{m}$ thick SiO_2 doped with Ge, which can increase the refractive index of the waveguide core, was deposited by plasma-enhanced chemical vapor deposition (PECVD). A $6 \mu\text{m}$ wide core was processed by lithography and the dry etch technique; this size can support single-mode transmission. Then, the top cladding layer was covered with borophosphosilicate glass (BPSG), which can be used to make the refractive index of the top cladding equal to that of the bottom cladding. The thickness of the top and bottom layer was $15 \mu\text{m}$, which can reduce the leakage loss of the cladding layer. The wafer was annealed after each process to realize stress compensation and reduce polarization-dependent loss caused by birefringence. Finally, a layer of glass was covered on the top cladding for protecting the connection and packaging between the waveguides and the optical fiber. In order to carry out the comparison test, three groups of resonators with different gaps were fabricated ($g_1 = 6.9 \mu\text{m}$, $g_2 = 6.7 \mu\text{m}$; $g_1 = g_2 = 6.9 \mu\text{m}$; and $g_1 = g_2 = 6.7 \mu\text{m}$).

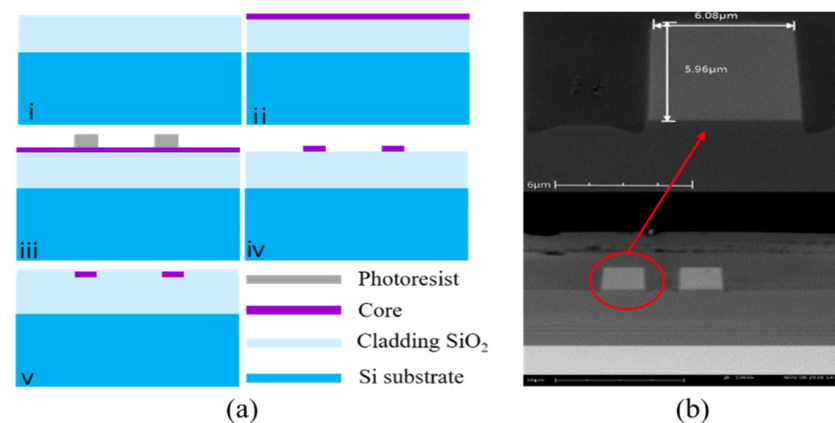


Figure 2. (a) Schematic of key fabrication and process steps of the resonator: (i) SiO_2 of the bottom cladding layer by being thermally grown; (ii) core layer by PECVD; (iii) ultraviolet lithography; (iv) dry etch; and (v) SiO_2 of the bottom cladding layer by PECVD. (b) SEM image of a coupling region cross-section.

4. Experiment

The experimental test system was built up to measure the resonance spectrum of the transmissive silica waveguide ring resonator (Figure 3a). A tunable laser with a central wavelength of 1550 nm and a spectral linewidth of 300 KHz was used as an incident light source. A triangular voltage signal was applied to the laser for the linear scanning of the laser frequency. An isolator was placed between the laser and the resonator in order to avoid the laser from being influenced by the echo light. The light was then coupled into the resonator. A photodetector was used to convert the light output from the resonator into an electrical signal. The resonance spectrum could be observed on the oscilloscope.

Based on the above system, an experimental testing system of a resonant micro-optic gyroscope based on a transmissive silica waveguide ring resonator in an output loop state was established (Figure 3b). A Y-branch multifunctional phase modulator made of proton exchange lithium niobate was used to modulate the optical signals. The modulated signals entered into the resonator from the two input ports; the two light waves were transmitted around the circular waveguide in opposite directions and then outputted to the photodetectors, PD1 and PD2, from the two drop ports of the resonator.

Because of the structural advantages of the transmissive resonator compared with the reflective resonator, there was no need to use the circulators. The photodetectors converted the light intensity signals into current signals, which were then converted into voltage signals by transimpedance amplifiers. The demodulated signal from a lock-in amplifier (LIA1) was used to supply feedback to the frequency locking module to lock the laser’s central frequency to the resonance point of the resonator through a PI controller, and the other demodulated signal from LIA2 was used as the gyroscope output signal. The data acquisition and signal processing of the frequency-locked loop and the output loop were realized with Field Programmable Gate Array (FPGA).

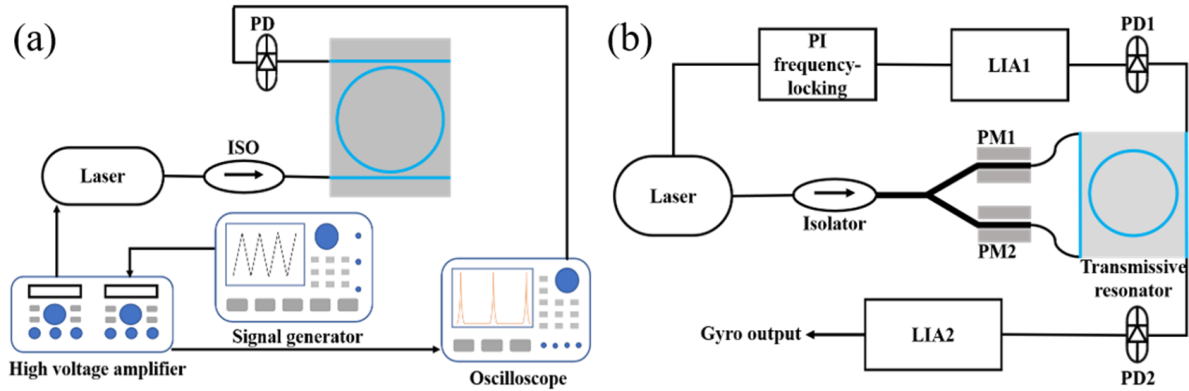


Figure 3. (a) Schematic diagram of the test system for the resonator; (b) schematic diagram of the gyroscope test system.

5. Results

The resonant curve of the drop port of the transmissive resonator ($g_1 = 6.9 \mu\text{m}$ and $g_2 = 6.7 \mu\text{m}$) after Lorentz fitting is shown in Figure 4. The black curve refers to the resonant spectrum and the red curve indicates the output voltage of the triangle wave sweep signal. The corresponding scan voltage difference was 0.615 V. The frequency modulation coefficient of the laser was 15 MHz/V; therefore, we determined that the FWHM of the resonator was 9.22 MHz. Furthermore, we calculated that the Q was 2.1×10^7 and the finesse was 119.

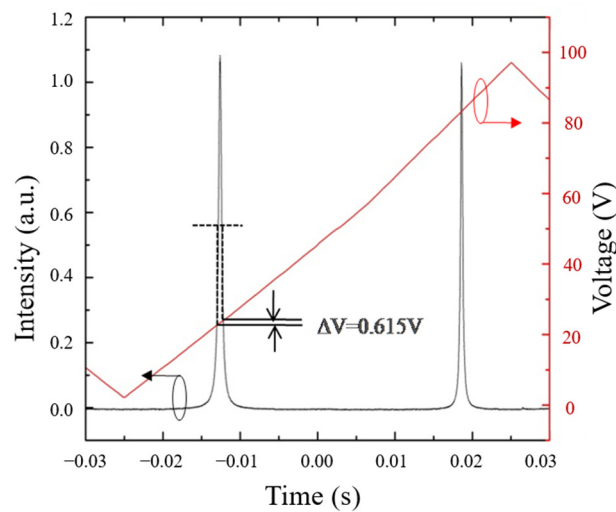


Figure 4. Curve fitting of the resonant spectrum ($g_1 = 6.9 \mu\text{m}$ and $g_2 = 6.7 \mu\text{m}$).

The transmissive resonators with different parameters were connected to the gyroscope system for rotation tests. Step signals from the gyroscope system could be obtained by adjusting the rotating speed of the rotary table with $\pm 20^\circ/\text{s}$, $\pm 40^\circ/\text{s}$, $\pm 60^\circ/\text{s}$, and $\pm 80^\circ/\text{s}$, respectively, as shown in Figure 5a. Then, the scale factor of the resonant optical gyroscope system based on the transmissive resonator was calculated by the least square method, as shown in Figure 5b.

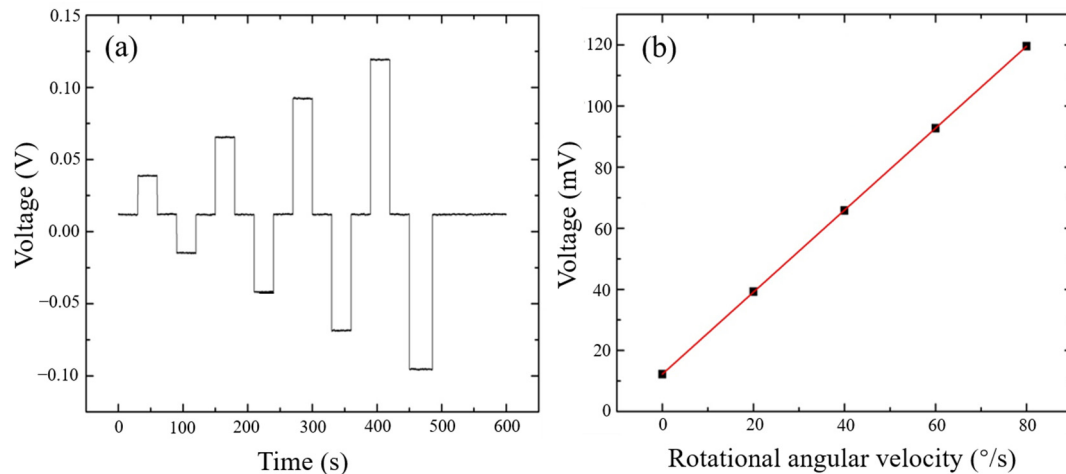


Figure 5. (a). Rotation step signals; (b) least square fitting ($g_1 = 6.9 \mu\text{m}$ and $g_2 = 6.7 \mu\text{m}$).

According to the above test steps, the quality factor, finesse, and scale factors of the gyroscope system of the three transmissive optical waveguide resonators with different parameters were tested, respectively. The results are shown in Table 1.

Table 1. Quality factors and scale factors of resonators with different parameters tested by the experiment.

g_1 (μm)	g_2 (μm)	Quality Factor	Scale Factor ($\text{mV}/^\circ/\text{s}$)
6.9	6.7	2.1×10^7	1.34
6.9	6.9	1.5×10^7	0.79
6.7	6.7	1.2×10^7	0.69

The resonant micro-optic gyroscope based on a transmissive silica waveguide ring resonator with optimal parameters was tested at room temperature on a static table. A minimum of Allan deviation with $122^\circ/\text{h}$ over a one-hour test was successfully demonstrated (see Figure 6). Then, a bias stability of $183.7^\circ/\text{h}$ was calculated by dividing the minimum Allan deviation by 0.664 [22]. The bias stability of the other two groups of resonators were $191.7^\circ/\text{h}$ ($g_1 = 6.9 \mu\text{m}$ and $g_2 = 6.9 \mu\text{m}$) and $203.1^\circ/\text{h}$ ($g_1 = 6.7 \mu\text{m}$ and $g_2 = 6.7 \mu\text{m}$). The test results show that the gyro index of the resonator ($g_1 = 6.9 \mu\text{m}$ and $g_2 = 6.7 \mu\text{m}$) is best, and the test results were consistent with the simulation results.

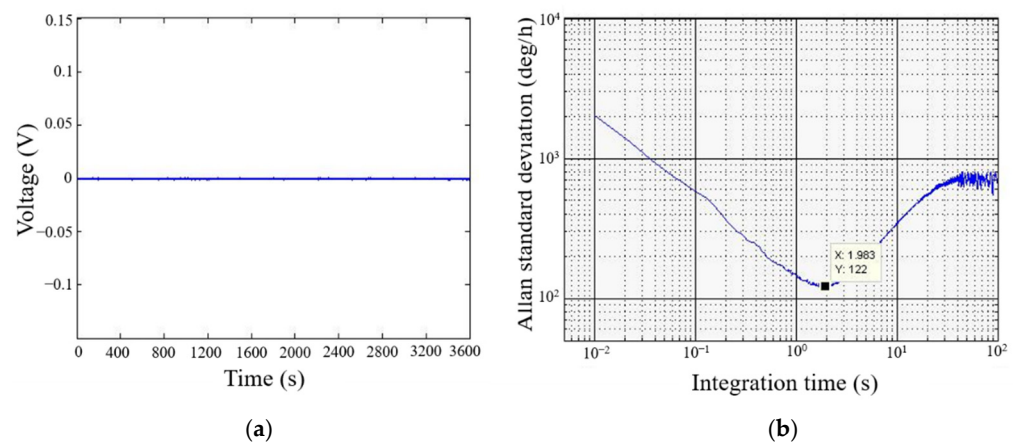


Figure 6. (a) One-hour static test result; (b) Allan standard deviation of the rotation data ($g_1 = 6.9 \mu\text{m}$ and $g_2 = 6.7 \mu\text{m}$).

6. Conclusions

We designed and fabricated a transmissive silica waveguide ring resonator with various gaps. The modeling of a transmissive resonator used in a micro-optic gyroscope was carried out, and the relationship between the resonator's transmission coefficient and the gyroscope's sensitivity was identified. A scale factor of $1.34 \text{ mV}/^\circ/\text{s}$ was achieved using an open-loop system, which was the highest value attained among all the resonators that we fabricated; this result was consistent with those of the simulations. The quality of the resonator was up to 2.1×10^7 , which is the highest quality among the reported transmissive resonators. A bias stability of $183.7^\circ/\text{h}$ over a one-hour test was successfully demonstrated, which is the best index of the optical gyroscope, based on the silicon dioxide transmissive resonators. The results show that our design method is feasible and provides ideas for the design of high quality transmissive optical waveguide resonators. In addition, the quality factor, finesse, and zero-bias stability of the gyroscope were close to those of the reflective resonator with nearly the same size. This provides a sound foundation for the improvement of the micro-optic gyroscope.

Author Contributions: Conceptualization, W.Z. and W.L.; methodology, H.G.; software, W.Z.; validation, J.T., W.L. and W.Z.; writing—original draft preparation, W.Z.; writing—review and editing, W.Z.; supervision, J.T.; funding acquisition, J.L. All authors have read and agreed to the published version of the manuscript.

Funding: This research was funded by the National Natural Science Foundation of China (No. 51727808, 51821003 and 51922009).

Conflicts of Interest: The authors declare no conflict of interest.

References

1. Ciminelli, C.; Dell'Olio, F.; Campanella, C.; Armenise, M.N. Photonic technologies for angular velocity sensing. *Adv. Opt. Photon.* **2012**, *2*, 370–404. [[CrossRef](#)]
2. Dell'Olio, F.; Indiveri, F.; Innone, F.; Russo, P.D.; Ciminelli, C.; Armenise, M. System test of an optoelectronic gyroscope based on a high Q-factor InP ring resonator. *Opt. Eng.* **2014**, *53*, 127104. [[CrossRef](#)]
3. Guillén-Torres, M.; Cretu, E.; Jaeger, N.A.F.; Chrostowski, L. Ring resonator optical gyroscopes-parameter optimization and robustness analysis. *J. Light. Technol.* **2012**, *30*, 1802–1817. [[CrossRef](#)]
4. Kalantarov, D.; Search, C.P. Effect of input–output coupling on the sensitivity of coupled resonator optical waveguide gyroscopes. *J. Opt. Soc. Am. B* **2013**, *30*, 377–381. [[CrossRef](#)]
5. Ma, H.; Zhang, J.; Wang, L.; Lu, Y.; Ying, D.; Jin, Z. Resonant micro-optic gyro using a short and high-finesse fiber ring resonator. *Opt. Lett.* **2015**, *40*, 5862–5865. [[CrossRef](#)] [[PubMed](#)]
6. Jin, Z.; Zhang, G.; Mao, H.; Ma, H. Resonator micro optic gyro with double phase modulation technique using an FPGA-based digital processor. *Opt. Commun.* **2012**, *285*, 645–649. [[CrossRef](#)]
7. An, P.; Zheng, Y.; Yan, S.; Xue, C.; Wang, W.; Liu, J. High-Q microsphere resonators for angular velocity sensing in gyroscopes. *Appl. Phys. Lett.* **2015**, *106*, 327. [[CrossRef](#)]

8. Wang, J.; Feng, L.; Wang, Q. Reduction of angle random walk by in-phase triangular phase modulation technique for resonator integrated optic gyro. *Opt. Express* **2016**, *24*, 5463–5468. [[CrossRef](#)] [[PubMed](#)]
9. Mao, H.; Ma, H.; Jin, Z. Polarization maintaining silica waveguide resonator optic gyro using double phase modulation technique. *Opt. Express* **2011**, *19*, 4632–4643. [[CrossRef](#)] [[PubMed](#)]
10. Dell’Olio, F.; Conteduca, D.; Ciminelli, C.; Armenise, M.N. New ultrasensitive resonant photonic platform for label-free biosensing. *Opt. Express* **2015**, *23*, 28593–28604. [[CrossRef](#)] [[PubMed](#)]
11. Chang, X.; Ma, H.; Jin, Z. Resonance asymmetry phenomenon in waveguide-type optical ring resonator gyro. *Opt. Commun.* **2012**, *285*, 1134–1139. [[CrossRef](#)]
12. Spencer, D.T.; Bauters, J.F.; Heck, M.J.R.; Bowers, J.E. Integrated waveguide coupled Si₃N₄ resonators in the ultrahigh-Q regime. *Optica* **2014**, *1*, 153–157. [[CrossRef](#)]
13. Qian, K.; Tang, J.; Guo, H.; Liu, W.; Liu, J.; Xue, C.; Zheng, Y.; Zhang, C. Under-coupling whispering gallery mode resonator applied to resonant micro-optic gyroscope. *Sensors* **2017**, *17*, 100. [[CrossRef](#)] [[PubMed](#)]
14. Vannahme, C.; Suche, H.; Reza, S. Integrated optical Ti:LiNbO₃ ring resonator for rotation rate sensing. In Proceedings of the 13th European Conference on Integrated Optics (ECIO), Copenhagen, Denmark, 25–27 April 2007.
15. Ciminelli, C.; D’Agostino, D.; Carnicella, G.; Dell’Olio, F.; Conteduca, D.; Ambrosius, H.P.M.M.; Smit, M.K.; Armenise, M.N. A high-Q InP resonant angular velocity sensor for a monolithically integrated optical gyroscope. *IEEE Photon. J.* **2015**, *8*, 6800418. [[CrossRef](#)]
16. Wang, J.; Feng, L.; Wang, Q.; Jiao, H.; Wang, X. Suppression of backreflection error in resonator integrated optic gyro by the phase difference traversal method. *Opt. Lett.* **2016**, *41*, 1586–1589. [[CrossRef](#)] [[PubMed](#)]
17. Haavisto, J.; Pajer, G.A. Resonance effects in low-loss ring waveguides. *Opt. Lett.* **1980**, *5*, 510–512. [[CrossRef](#)] [[PubMed](#)]
18. Ma, H.; Chen, Z.; Yang, Z.; Yu, X.; Jin, Z. Polarization-induced noise in resonator fiber optic gyro. *Appl. Opt.* **2012**, *51*, 6708–6717. [[CrossRef](#)] [[PubMed](#)]
19. Feng, L.; Wang, J.; Zhi, Y.; Tang, Y.; Wang, Q.; Li, H.; Wang, W. Transmissive resonator optic gyro based on silica waveguide ring resonator. *Opt. Express* **2014**, *22*, 27565–27575. [[CrossRef](#)] [[PubMed](#)]
20. Poon, J.K.S.; Scheuer, J.; Mookherjee, S.; Paloczi, G.T.; Huang, Y.; Yariv, A. Matrix analysis of microring coupled-resonator optical waveguides. *Opt. Express* **2004**, *12*, 90–103. [[CrossRef](#)] [[PubMed](#)]
21. Ying, D.; Wang, Z.; Mao, J.; Jin, Z. An open-loop RFOG based on harmonic division technique to suppress LD’s intensity modulation noise. *Opt. Commun.* **2016**, *378*, 10–15. [[CrossRef](#)]
22. Matejček, M.; Šostronek, M. New experience with Allan variance: Noise analysis of accelerometers. In Proceedings of the Communication and Information Technologies (KIT), Vysoké Tatry, Slovakia, 4–6 October 2017; pp. 1–4.